Turkish Journal of Electrical Engineering & Computer Sciences

http://journals.tubitak.gov.tr/elektrik/

Research Article

Turk J Elec Eng & Comp Sci
(2018) 26: 1612 – 1622

doi:10.3906/elk-1709-54

Adaptive collaborative speed control of PMDC motor using hyperbolic secant functions and particle swarm optimization

Omer SALEEM[1,*], **Khalid MAHMOOD-UL-HASAN**[2]

[1]Department of Electrical Engineering, National University of Computer and Emerging Sciences, Lahore, Pakistan
[2]Department of Electrical Engineering, University of Engineering and Technology, Lahore, Pakistan

Received: 06.09.2017 • **Accepted/Published Online:** 01.01.2018 • **Final Version:** 30.05.2018

Abstract: This paper presents an adaptive collaborative speed controller for a permanent magnet direct-current (PMDC) motor. The proposed scheme beneficially combines the control efforts of a proportional-integral (PI) controller and a linear-quadratic regulator (LQR) via a weighted summing module. Initially, the weightages of the summing module are kept fixed. They are optimally tuned and tested via the particle swarm optimization algorithm. In order to synergize the controller combination, these weightages are adaptively modulated as well, using hyperbolic secant functions of the error dynamics of the motor's angular speed. The adaptive combination renders significant enhancement in the transient response, steady-state response, input-energy consumption, disturbance rejection, and variable load-torque handling capability of the motor. The adaptive-weighted controller is tested against the PI controller, the LQR, and a fixed-weighted collaborative controller via 'hardware-in-the-loop' experiments. The experimental results are presented to validate the robustness of the adaptive controller.

Key words: PMDC motor, linear-quadratic regulator, PI controller, adaptive-weighted control, particle swarm optimization, hyperbolic secant function

1. Introduction

Permanent magnet direct-current (PMDC) motors are used in steel rolling mills, automobiles, conveyors, and various robotics applications due to their controllability, reliability, and low cost [1,2]. Extensive research has been done to synthesize optimal closed-loop speed controllers for high-precision and efficient motor drives [3–6]. Most of these schemes have a complex design. Owing to their design limitations, these controllers normally make a trade-off between various performance parameters of the system. However, the proportional-integral (PI) controllers and linear-quadratic regulators (LQRs) are still the most widely used schemes [7,8]. PI controllers are famous for optimizing the steady-state response. A well-tuned PI controller completely eliminates the small steady-state fluctuations and damps the oscillations (or overshoots) caused by random perturbations (or transients) in the response [9]. At the same time, however, the transient response gets significantly degraded. On the contrary, LQRs are optimal controllers that employ full state feedback to improve the error convergence rate and transition time of the response [10]. However, they inevitably exhibit overshoots and steady-state errors due to the lack of integral control. Moreover, the LQRs cannot compensate the modeling errors [11].

A lot of research is being done to enhance the speed control performance of DC motors by simply adding the control efforts of LQRs and PI controllers [12,13]. The combination can be further synergized by taking

*Correspondence: omer.saleem@nu.edu.pk

a weighted sum of the available control resources. However, the weightages must be optimally selected. In this research, for the sake of comparison, initial test trials are conducted by metaheuristically optimizing the weightages. Several metaheuristic algorithms have been discussed in the literature [14,15]. The particle swarm optimization (PSO) algorithm is used in this study because it is relatively easy to compute and converges quickly to deliver the global best solution [16]. The PI controller gains and the LQR penalty matrices are also tuned via the PSO algorithm. Although it is simple, the fixed-weighted sum of the individual control efforts does not consider all the system dynamics and hence may not always yield robust control performance. Apart from combining the benefits, it inevitably passes along the demerits of the constituent controllers in the overall control scheme. Furthermore, the system abruptly switches between the constituent controllers, which leads to oscillations in the system as it converges or diverges from the reference speed.

Therefore, in this study, a self-tuning mechanism is proposed to update the weightages [17]. A well-postulated self-tuning mechanism dynamically adjusts the weightages to deliver the best features offered by each controller while suppressing their demerits. The weightages can be self-tuned via neuro-fuzzy mechanisms [18], but they lack robustness against dynamic uncertainties due to their heuristic synthesis. The adaptation mechanisms based on nonlinear functions are simple and effective. Several nonlinear functions are proposed in literature, such as sigmoidal, hyperbolic, and piece-wise functions [19]. In this research, the weightages are adaptively tuned via hyperbolic secant functions (HSFs) of the error dynamics of the motor's speed [20]. These are symmetrical functions naturally bounded between 0 and 1.

The remainder of the paper is organized as follows. The experimental setup is described in Section 2. The theoretical background of LQRs and PI controllers is explained in Section 3. The proposed controller is synthesized in Section 4. Parameter optimization is described in Section 5. The experimental analysis of the controller performance is presented in Section 6. The paper is concluded in Section 7.

2. Experimental setup

The DC motor control trainer (DCMCT) by Quanser, shown in Figure 1, is used as a benchmark to test and validate the effectiveness of the proposed controller [21].

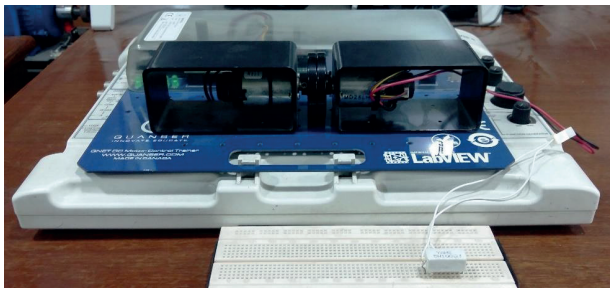

Figure 1. DC motor control trainer.

2.1. Hardware setup

The DCMCT setup consists of a PMDC motor that is equipped with a tachometer and current sensor to measure the angular velocity and the armature current drawn by the DC motor, respectively. The motor shaft is loaded with an inertial disk. The hardware transmits the analog sensor data to and receives the control commands from a LabVIEW-based graphical user interface via a serial communication link at 9600 bps [22]. The sampling frequency used in this research is 500 Hz.

2.2. Mathematical model of motor

The differential equations representing the mechanical and electrical characteristics of the motor are given by Eqs. (1) and (2), respectively [23].

$$J_M \frac{d\omega_r}{dt} + B\omega_r = K_t i_a \tag{1}$$

$$L_a \frac{di_a}{dt} + R_a i_a = V_m - K_t \omega_r \tag{2}$$

The state-space model of a dynamical system is generally given by Eqs. (3) and (4).

$$\frac{dx}{dt} = Ax + Bu \tag{3}$$

$$y = Cx + Du \tag{4}$$

Here, x is the state vector, y is the output vector, u is the control input signal, A is the system transition matrix, B is the input matrix, C is the output matrix, and D is the feedforward matrix. These matrices are described in Eq. (5).

$$x = \begin{bmatrix} \omega_r & i_a \end{bmatrix}^T, u = V_m, A = \begin{bmatrix} \frac{-B}{J_M} & \frac{K_t}{J_M} \\ \frac{-K_t}{L_a} & \frac{-R_a}{L_a} \end{bmatrix}, B = \begin{bmatrix} 0 \\ \frac{1}{L} \end{bmatrix}, C = \begin{bmatrix} 1 & 0 \end{bmatrix}, D = 0 \tag{5}$$

Here, ω_r is the motor's actual speed, i_a is the armature current, and V_m is the motor's terminal voltage. To observe the load-torque characteristics of the motor, its shaft is coupled with a DC mini generator that is connected to an electrical load resistance, as shown in Figure 2. The remaining system parameters are identified in Table 1.

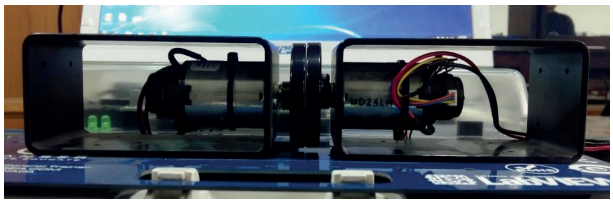

Figure 2. Expanded view of the motor/generator coupling.

3. Theoretical background

This section provides the theoretical background of conventional motor speed controllers.

3.1. Proportional-integral controller

The PI controller is a widely favored model-free control technique [24]. It is preferred due to its simple structure and effective controlling ability. Derivative action is neglected because it tends to significantly amplify high-frequency noise signals as well. The PI controller is a linear combination of the instantaneous value of error, as shown in Eq. (6), and the integral of errors. The weightages of the error and the integral of error are referred to as the proportional (k_p) and integral (k_i) gains, respectively. The associated control law is given by Eq. (7).

$$e_\omega = \omega_d - \omega_r \tag{6}$$

Table 1. Electromechanical parameters of the experimental setup.

System	Parameters	Symbol	Values
PMDC motor	Armature resistance	R_a	3.3 Ω
	Armature inductance	L_a	0.047 H
	Maximum torque	$T_{\max}$	0.14 Nm
	Torque constant	K_t	0.028 Nm/A
	Motor inertia	J_M	9.64×10^{-6} kgm^2
	Friction coefficient	B	1.18×10^{-5} Nms
	Supply voltage	V_S	±24.0 V
	Maximum input current	I_S	5.0 A
	Inertial load disk mass	m_{disc}	0.062 kg
	Inertial load disk radius	r_{disc}	0.0242 m
Generator	Rated voltage	V_G	12 V
	Load resistance	R_L	120 Ω, 5.0 W

$$u_{pi} = k_p e + k_i \int_0^T e \, d\tau \tag{7}$$

Here, ω_d represents the motor's reference speed. Poorly tuned gains cause unrecoverable oscillations in the response. Hence, the PI gains are optimally tuned via the PSO algorithm (see Section 5).

3.2. Linear quadratic regulator

The LQR uses the linear state-space model of a dynamical system along with its full state feedback to minimize a quadratic performance index in order to deliver optimal control decisions [25]. The quadratic performance-index is expressed in Eq. (8).

$$J_q = \int_0^T x^T Q x + u_{lqr}^T R u_{lqr} \, dt \tag{8}$$

Here, Q and R denote the state- and control-penalty matrices, respectively. Matrix Q is positive semidefinite and R is positive-definite. The penalty matrices are generally expressed according to Eq. (9).

$$Q = \begin{bmatrix} q_{11} & 0 \\ 0 & q_{22} \end{bmatrix}, \quad R = r \tag{9}$$

In this study, matrices Q and R are optimally tuned via the PSO algorithm (see Section 5). The state-feedback control law is given by Eq. (10).

$$u_{lqr} = -Kx \tag{10}$$

Here, K is denoted as the state-feedback gain vector. The gain vector, expressed in Eq. (11), relocates the system's open-loop poles to synthesize an optimal controller.

$$K = R^{-1} B^T P \tag{11}$$

Here, P is a symmetric positive-definite matrix that is evaluated by solving the algebraic Riccati equation, shown in Eq. (12).

$$A^T P + PA - PBR^{-1}B^T P + Q = 0 \tag{12}$$

Owing to the quadratic nature of the performance index, the applied control signal is proportional to the square of state variations; therefore, if the variations are large, the minimization is faster and the LQR system converges quickly to deliver optimal control decisions. This phenomenon significantly improves the transient response. The optimized gain vector, K, used in this study is given by Eq. (13).

$$K = \begin{bmatrix} 1.168 & -0.277 \end{bmatrix} \tag{13}$$

4. Collaborative speed control strategy

In this section, two different mechanisms are proposed to beneficially combine the outputs of LQR- and PI-based speed-controllers via a WSM. Both of these mechanisms are implemented by using the same LQR and PI controllers that were synthesized in the previous section. The main objective is to optimize the transient as well as the steady-state response of the motor speed, even in the presence of bounded exogenous disturbances. In order to utilize the benefits offered by each controller and suppress their demerits, the LQR and PI controller outputs are linearly combined, using Eq. (14), to generate better control decisions [26].

$$u = (h)\, u_{pi} + (1 - h)\, u_{lqr} \tag{14}$$

Here, h and $1 - h$ are the weightages of the linear combination, such that $h \in [0, 1]$.

4.1. Fixed-weighted collaborative speed controller

The fixed-weighted collaborative speed controller (FCSC) combines the LQR and the PI controllers via the weighted linear combination given by Eq. (14). The value of h is optimally tuned via the PSO algorithm (see Section 5) and is kept fixed throughout the experimental trials. The FCSC block diagram is shown in Figure 3.

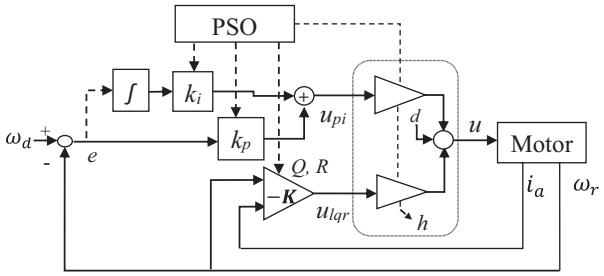

Figure 3. Fixed-weighted collaborative speed controller (FCSC).

4.2. Adaptive collaborative speed controller

In order to further synergize the performance of the weighted combination of the LQR and PI controller, h is adaptively modulated with the aid of a self-tuning mechanism. The proposed mechanism employs HSFs of error and change of error in angular speed to adaptively tune h [27]. The dynamic adjustment of WSM weightage with respect to the variations in error only, as shown in [17], is not sufficient to eliminate the effects of exogenous disturbances and parametric uncertainties. Therefore, the proposed mechanism updates the value of h by selecting the maximum of the two instantaneous values provided by the functions, g_1 and g_2, as shown in Eq. (15).

$$h = max\ (g_1\ ,\ g_2) \tag{15}$$

Here, g_1 and g_2 are HSFs of the error and derivative of error in ω_r, given by Eq. (16).

$$g_1 = \sec h\,(\alpha_1 e_\omega)\ ,\ \ g_2 = \sec h\,(\alpha_2 \dot{e}_\omega) \tag{16}$$

Here, α_1 and α_2 denote the variation rates of the functions g_1 and g_2, respectively. They determine the variance of the HSF, as shown in Figure 4. The variation rates of HSFs are optimally tuned via the PSO algorithm as well (see Section 5). Once the HSFs are equipped with optimized variation rates, they serve to effectively adjust the value of h with time.

The adaptive collaborative speed controller (ACSC) is shown in Figure 5. When the error abruptly increases during the transient or impulsive disturbance conditions, the weightages are quickly adjusted to increase the contribution of the LQR. As the error recedes, the weightages are adaptively readjusted to systematically increase the contribution of the PI controller in order to enhance the motor's steady-state response.

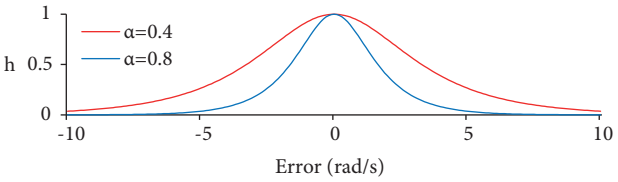

Figure 4. Variation pattern of hyperbolic secant function.

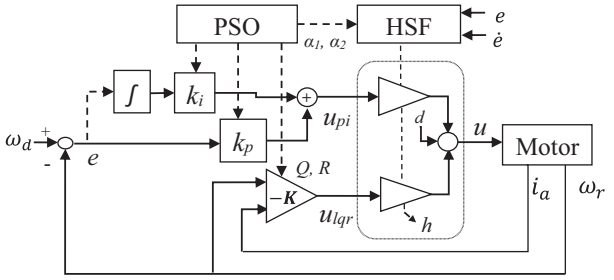

Figure 5. Adaptive collaborative speed controller (ACSC).

5. Particle swarm optimization

The PSO algorithm is a popular metaheuristic population-based stochastic optimization technique [28]. Initially a random population of candidate solutions, called 'particles', is selected for each parameter that needs to be tuned. The PSO algorithm searches the entire population to explore and converge to the global best solution. Each particle has a position and velocity associated to it. The expressions used to update the velocity (V_i) and position (X_i) of a particle I are given by Eqs. (17) and (18), respectively.

$$V_i = w_i V_i + c_1 r_1\,(P_i - X_i) + c_2 r_2\,(P_g - X_i) \tag{17}$$

$$X_i = X_i + V_i \tag{18}$$

Here, c_1 and c_2 are the cognitive coefficients, r_1 and r_2 are random real numbers in the interval [0, 1], and w is the inertia weight. In this study, the PSO algorithm is used to optimally tune and fix the PI gains (k_p and k_i), the LQR penalty-matrices (Q and R), the weightage (h) in the FCSC, and the variation rates of HSFs (α_1 and α_2) in the ACSC. The values of the cognitive coefficients (c_1 and c_2) selected are 2.04 and 2.18, respectively. The fitness value of each particle is computed via the function given in Eq. (19).

$$Fitness = \frac{1}{(OS)^2 + (t_r)^2 + (t_s)^2 + \int_0^T (e)^2 + 0.01\,(V_m)^2\,d\tau} \tag{19}$$

Here, t_r is the rise time, OS is the overshoot, and t_s is the time taken by the response to settle within $\pm 5\%$ of the reference speed. The evaluated fitness value of each particle is recorded and compared with the best fitness value, also known as the local best (P_i), available so far. If a higher fitness value is achieved then it is set as the new P_i. The particle with the highest fitness value among all the particles in the population is chosen as the global best (P_g). The inertia weight (w) of the optimizer, given by Eq. (20), decreases from 1 to 0 in order to converge to the global best solution.

$$w_j = w_{\max} - \left(\frac{w_{\max} - w_{\min}}{j_{\max}} \right) j \tag{20}$$

Here, j is the current number of iterations, $j_{\max}$ is the maximum allowable number of iterations, and the values of $w_{\min}$ and $w_{\max}$ are selected as 0.394 and 0.902, respectively. After each iteration, the fitness of the parameters is checked to decide their convergence to the P_g value. The flow of the PSO algorithm is diagrammatically illustrated in Figure 6. A sample size of 100 candidate solutions is taken for the optimization of each parameter. The optimized parameter values, the range of values selected for optimization of each parameter, the fitness of optimized parameters, and the number of iterations taken by them to converge to the P_g value are provided in Table 2. The variations in the convergence behavior of the parameters over the subsequent iterations of the optimization process are clearly presented in Figure 7.

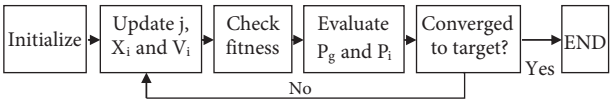

Figure 6. Flowchart of PSO algorithm.

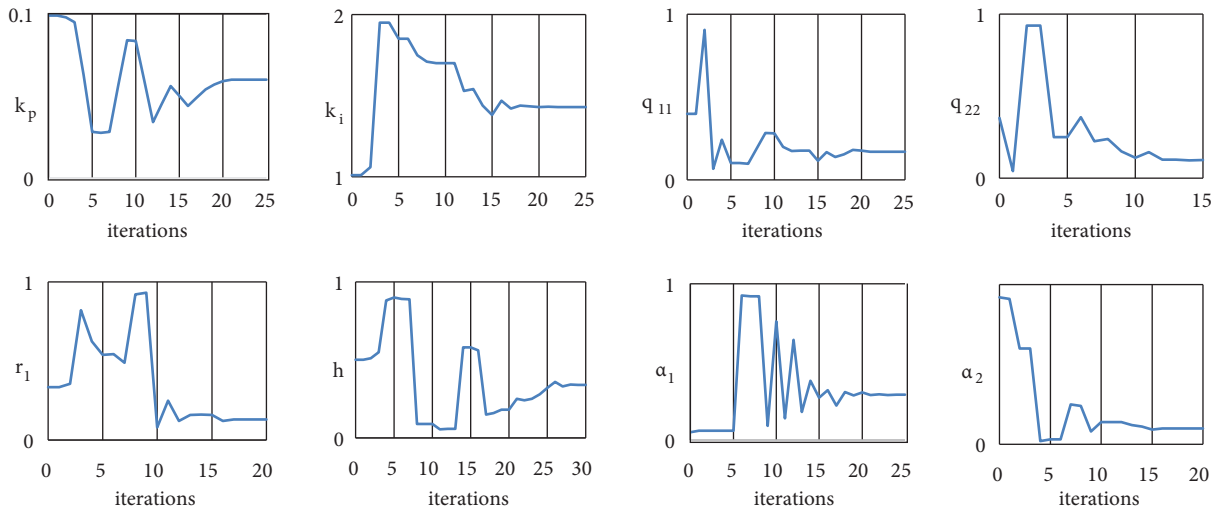

Figure 7. Variation in the parameters along the optimization process.

6. Tests and results

The performance of the ACSC is compared with the PI controller, LQR, and FCSC. The following test cases are conducted on the DCMCT via 'hardware-in-the-loop' experiments.

Table 2. Summary of optimized parameters.

Controller	PI		LQR			FCSC	ACSC	
Parameter	k_p	k_i	q_{11}	q_{22}	r	h	α_1	α_2
Value	0.06	1.43	0.17	0.11	0.13	0.34	0.29	0.01
Range	[0, 1]	[1, 2]	[0, 1]	[0, 1]	[0, 1]	[0, 1]	[0, 1]	[0, 0.1]
Fitness ($\times 10^{-3}$)	0.131	0.392	0.032	0.025	0.026	5.431	3.722	4.233
Iterations	22	19	21	12	18	28	23	17

Test case A: A step input of 100 rad/s is applied to the motor. The resulting variations in ω_r for each controller are shown in Figure 8. The expanded view of the steady-state response is shown in Figure 9. The variations in h for the ACSC are shown in Figure 10. The test results are recorded in Table 3. The LQR gives the best transient response but a poor steady-state performance, since it lacks integral control and proper damping. The converse is true for the PI controller. The transient response exhibited by the FCSC is better than that of the PI controller but poorer than that of the LQR. Similarly, the steady-state response of the FCSC surpasses that of the LQR but lags behind the PI controller. The ACSC outperforms the other aforementioned controllers.

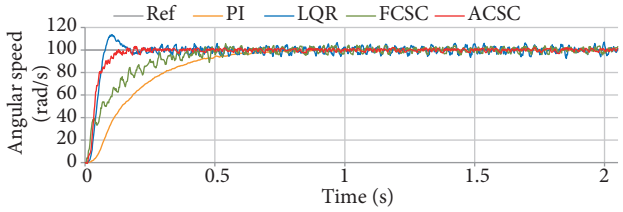

Figure 8. Step response of speed controllers without disturbance.

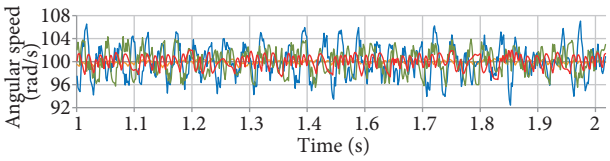

Figure 9. Zoomed steady-state response of speed controllers.

Table 3. Summary of test results.

Controller	Test A					Test B		Test C	
	t_r (s)	OS (%)	t_s (s)	E_{ss} (rad/s)	$\int V_m^2 dt$ (V^2)	MAE (rad/s)	(rad/s)	MAE (rad/s)	t_s (s)
PI	0.43	0.57	0.60	0.39	244.82	21.96	0.30	8.84	0.79
LQR	0.12	13.70	0.23	3.52	279.23	26.06	0.08	29.06	0.22
FCSC	0.29	5.61	0.40	2.17	258.77	20.10	0.21	20.08	0.31
ACSC	0.14	3.06	0.16	0.91	267.14	15.83	0.10	11.04	0.29

E_{ss} = Root-mean-square of steady-state error, MAE = maximum absolute error.

Test case B: An impulsive disturbance signal (d), of +1.0 V magnitude and 0.02 s duration, is applied at the controller's output at t = 1.6 s to perturb the steady-state response of the motor. The variations occurring in ω_r are illustrated in Figure 11. The variations in h for ACSC are shown in Figure 12. As demonstrated in Table 3, the LQR response converges quickly to the reference while exhibiting the largest error variation. The PI controller has the slowest convergence rate. The FCSC shows a slight improvement. The ACSC shows the best disturbance rejection capability of all.

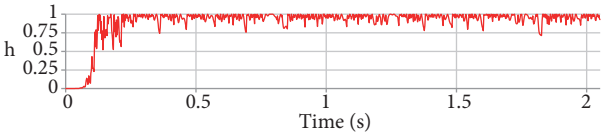

Figure 10. Variations in the value of h of the ACSC.

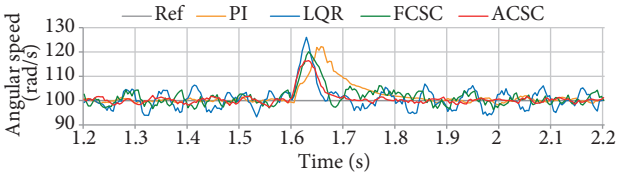

Figure 11. Effect of bounded impulsive disturbance on speed controllers.

Test case C: The motor's steady-state response is disturbed by changing its load torque in order to analyze the controller's reference tracking capability. The motor shaft is coupled with a loaded generator, as shown in Figure 2. The generator is switched on at t = 1.2 s. The variations in ω_r are illustrated in Figure 13. The variations in h for the ACSC are shown in Figure 14. The results in Table 3 demonstrate that The ACSC exhibits relatively smaller deviation from the reference and a faster error convergence rate.

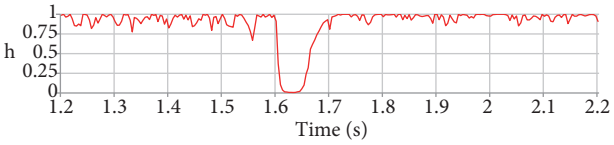

Figure 12. Variations in the value of h of the ACSC under impulsive disturbance.

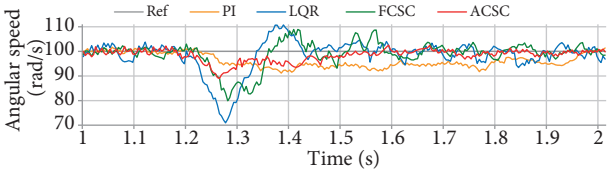

Figure 13. Effect of load torque changes on speed controllers.

Test case D: The performance of the ACSC is analyzed for different motor armature resistances (R_a). In order to emulate changes in R_a, an external resistance (R_e) is connected in series with the motor terminals. The responses exhibited by the ACSC, corresponding to a 100 rad/s step input, for four different values of R_e (0 Ω, 1.0 Ω, 1.5 Ω, and 1.8 Ω) are shown in Figure 15. The robustness of the ACSC against parametric variations in the motor is validated by the test results summarized in Table 4. The electrical damping slightly increases the transitional delays in the response.

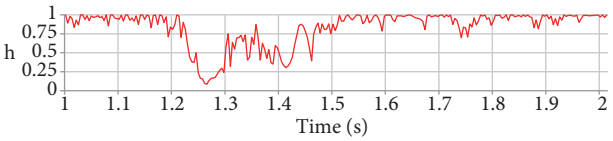

Figure 14. Variations in the value of h of the ACSC under load torque changes.

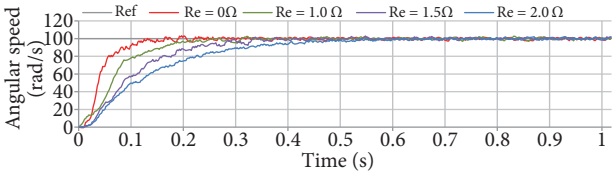

Figure 15. Step response of the ACSC with electrical damping.

Table 4. Summary of test results of the ACSC for electrical damping.

R_e (Ω)	t_r (s)	OS (%)	t_s (s)	E_{ss} (rad/s)	$\int V_m^2 dt$ (V^2)
0.0	0.14	3.06	0.16	0.91	267.14
1.0	0.20	2.91	0.25	0.89	274.24
1.5	0.26	2.72	0.33	0.89	283.65
2.2	0.36	2.26	0.52	0.88	289.56

7. Conclusion

This research presents a simple yet robust adaptive-weighted speed control system for a PMDC motor. The proposed scheme linearly combines the individual control efforts delivered by a PI controller and LQR. The weightages of the linear combination are self-tuned via HSFs of error dynamics in order to enhance the controller's error convergence rate and robustness against uncertainties. The nonlinear adaptive weighted mechanism appropriately utilizes the best control features offered by each controller. The LQR enhances the convergence rate, whereas the PI controller eliminates the steady-state fluctuations. The ACSC beneficially combines the best features offered by these controllers. It quickly converges to the reference speed while exhibiting minimum overshoot and oscillations. The dynamic adjustment of the weightages renders a smoother commutation between the constituent controllers and thus enables the ACSC to effectively and efficiently compensate the effects of exogenous disturbances, load torque variations, and parametric changes. The experimental performance of the ACSC is reasonably consistent with the optimality and robustness exhibited by advanced hybrid control schemes, such as fuzzy logic and sliding mode controllers [4]. In the future, the weighted-adaptive combination of other nonlinear and model-based control schemes can also be investigated to optimize the motor's speed control performance.

References

[1] Rajesh D, Ravikumar D, Bharadwaj SK, Vastav BKS. Design and control of digital DC drives in steel rolling mills. In: 2016 International Conference on Inventive Computation Technologies; 26–27 August 2016; Coimbatore, India. New York, NY, USA: IEEE. pp. 1-5.

[2] Khooban MH, Shasadeghi M, Niknam T, Blaabjerg F. Analysis, control and design of speed control of electric vehicles delayed model: multiobjective fuzzy fractional-order $PI^{\lambda}D^{\mu}$ controller. IET Sci Meas Technol 2017; 11: 249-261.

[3] Dal M. Enhancing sliding mode control with proportional feedback and feedforward: an experimental investigation on speed sensorless control of PM DC motor drives. Turk J Elec Eng & Comp Sci 2015; 23: 126-148.

[4] Ahmed H, Rajoriya A. A hybrid of sliding mode control and fuzzy logic control using a fuzzy supervisory switched system for DC motor speed control. Turk J Elec Eng & Comp Sci 2017; 25: 1993-2004.

[5] Kahveci H, Okumuş HI, Ekici M. Improved brushless DC motor speed controller with digital signal processor. IET Electron Lett 2014; 50: 864-866.

[6] Inoan I, Abrudean M. Control of an induction motor using the relay method approach. Control Eng Appl Inform 2014; 16: 13-22.

[7] Chebre M, Meroufel A, Bendaha Y. Speed control of induction motor using genetic algorithm-based PI controller. Acta Polytech Hungar 2011; 8: 141-153.

[8] Swargiary M, Dey J, Saha TK. Optimal speed control of induction motor based on linear quadratic regulator theory. In: 2015 Annual IEEE India Conference; 17–20 December 2015; New Delhi, India. New York, NY, USA: IEEE. pp. 1-6.

[9] Saleem O, Omer U. EKF-based self-regulation of an adaptive nonlinear PI speed controller for a DC motor. Turk J Elec Eng & Comp Sci 2017; 25: 4131-4141.

[10] Srivastaval S, Pandit VS. A scheme to control the speed of a DC motor with time delay using LQR-PID controller. In: 2015 International Conference on Industrial Instrumentation and Control; 28–30 May 2015; Pune, India. New York, NY, USA: IEEE. pp. 294-299.

[11] Ismail RMTR, Ahmad MA, Ramli MS. Speed control of buck-converter driven DC motor using LQR and PI: a comparative assessment. In: 2009 International Conference on Information Management and Engineering; 3–5 April 2009; Kuala Lumpur, Malaysia. New York, NY, USA: IEEE. pp. 651-656.

[12] Yassine B, Fatiha Z, Chrifi-Alaoui L. LQR-PI controller dedicated to the indirect vector control without speed sensor for an asynchronous motor. In: 2015 16th International Conference on Sciences and Techniques of Automatic Control & Computer Engineering; 21–23 December 2015; Monastir, Tunisia. New York, NY, USA: IEEE. pp. 634-640.

[13] Bagheri S, Jafarov T, Freidovich L, Sepehri N. Beneficially combining LQR and PID to control longitudinal dynamics of a SmartFly UAV. In: 2016 7th Annual Information Technology, Electronics and Mobile Communication Conference; 13–15 October 2016; Vancouver, Canada. New York, NY, USA: IEEE. pp. 1-6.

[14] Youns MD, Abdulla AI, Attya SM. Optimization control of DC motor with linear quadratic regulator and genetic algorithm approach. Tikrit J Eng Sci 2013; 20: 35-42.

[15] Navidi N, Bavafa M, Hesami S. A new approach for designing of PID controller for a linear brushless DC motor with using ant colony search algorithm. In: 2009 Asia-Pacific Power and Energy Engineering Conference; 27–31 March 2009; Wuhan, China. New York, NY, USA: IEEE. pp. 1-5.

[16] Kanojiya GR, Meshram PM. Optimal tuning of PI controller for speed control of DC motor drive using particle swarm optimization. In: 2012 International Conference on Advances in Power Conversion and Energy Technologies; 2–4 August 2012; Andhra Pradesh, India. New York, NY, USA: IEEE. pp. 1-6.

[17] Pedroso MD, Nascimento CB, Tusset AM, Kaster MS. A hyperbolic tangent adaptive PID + LQR control applied to a step-down converter using poles placement design implemented in FPGA. Math Probl Eng 2013; 2013: 101650.

[18] Zhou Y, Shang W, Liu M, Li X, Zeng Y. Simulation of PMSM vector control based on a self-tuning fuzzy PI controller. In: 8th International Conference on Biomedical Engineering and Informatics; 14–16 October 2015; Shenyang, China. New York, NY, USA: IEEE. pp. 609-613.

[19] Seraji H. A new class of non-linear PID controller with robotic applications. J Robot Syst 1998; 15: 161-181.

[20] Guo B, Hu L, Bai Y. A nonlinear PID controller with tracking differentiator applying in BLDCM servo system. In: 2012 7th International Power Electronics and Motion Control Conference; 2–5 June 2012; Harbin, China. New York, NY, USA: IEEE. pp. 2467-2471.

[21] Engle BJ, Watkins JM. A software platform for implementing digital control experiments on the Quanser DC motor control trainer. In: 2008 17th International Conference on Control Applications; 3–5 September 2008; Texas, USA. New York, NY, USA: IEEE. pp. 510-515.

[22] Abbas AN. Design and implementation of close loop DC motor speed control based on Labview. Int J Enhanc Res Eng Sci Technol 2014; 3: 354-361.

[23] Ruderman M, Krettek J, Hoffmann F, Bertram T. Optimal state space control of DC motor. In: 2008 17th World Congress of the International Federation of Automatic Control; 6–11 July 2008; Seoul, Korea. New York, NY, USA: IEEE. pp. 5796-5801.

[24] Ganzaroli CA, Carvalho DF, Dias RNHM, Reis MRC, Alves AJ, Domingos JL, Calixto WP. Heuristic and deterministic strategies applied on cascade PI controller tuning for speed control of a DC motor. In: 2015 CHILEAN Conference on Electrical, Electronics Engineering, Information and Communication Technologies; 28–30 October 2015; Santiago, Chile. New York, NY, USA: IEEE. pp. 101-106.

[25] Saisudha V, Seeja G, Pillay RV, Manikutty G, Bhavani RR. Analysis of speed control of DC motor using LQR method. Int J Control Theory Appl 2016; 9: 7377-7385.

[26] Pedroso MD, Nascimento CB, Tusset AM, Kaster MS. Performance comparison between nonlinear and linear controllers with weighted adaptive control applied to a buck converter using poles placement design. In: IEEE International Symposium on Industrial Electronics; 28–31 May 2013; Taipei, Taiwan. New York, NY, USA: IEEE, pp. 1-6.

[27] Isayed BM, Hawwa MA. A nonlinear PID control scheme for hard disk drive servosystems. In: 2007 15th Mediterranean Conference on Control & Automation; 27–29 July 2007; Athens, Greece. New York, NY, USA: IEEE. pp. 1-6.

[28] Salawria P, Lodhi RS, Nema P. Implementation of PSO-based optimum controller for speed control of BLDC motor. International Journal of Electrical, Electronics & Computer Science Engineering 2017; 6: 104-109.